# Kinetics of the Single-Crystal to Single-Crystal Two-Photon Photodimerization of α-*trans*-Cinnamic Acid to α-Truxillic Acid

**Jason B. Benedict* and Philip Coppens***

*Department of Chemistry, University at Buffalo, State University of New York, Buffalo, New York, 14260-3000*

*Received: October 16, 2008; Revised Manuscript Received: January 16, 2009*

The quadratic dependence of the rate of photodimerization of α-*trans*-cinnamic acid induced by 532 nm pulsed laser light confirms a two-photon mechanism in the single crystals. Single crystals in well-defined orientations and circularly polarized light were used in the experiments. The reaction rate deviates from first-order kinetics, but fits the JMAK expression with a coefficient indicating a mechanism intermediate between a random distribution of product molecules in the crystal and the existence of growing nuclei. The reaction is accompanied by a large change in the monoclinic $\beta$-angle of the unit cell, corresponding to increased $\pi$-overlap between adjacent molecules and therefore to an increased reaction rate. The improved penetration of the light in the crystal and more homogeneous product formation are significant advantages in studies of mechanisms of chemical reactions in single crystals.

## Introduction

It has recently been shown that two-photon excitation can dramatically increase the yield and/or the spatial homogeneity of the photoproducts within a crystal and increase the likelihood of single-crystal to single-crystal transformations.[1−3] In these studies pulsed laser sources with photon energies of approximately half the energy of the transition of interest are used to generate the desired photoproduct. An advantage of the two-photon technique is that because of the much lower absorption cross-section a crystal can be much more evenly exposed to light than is the case when excitation is by a single photon. In the latter case only the surface layer may be converted by the light.[2] The potential advantage of the technique is not limited to the study of chemical processes in crystals by steady-state methods, but may include time-resolved pump−probe experiments of molecular excited states and chemical reactions.[4−6]

However, the occurrence of a two-photon absorption process is not solely established by the energy of the photon absorbed, rather the relationship between the rate at which the photoproducts are generated and the intensity of the incident radiation must be examined.[7] Such a study has been performed for the photocleavage of coumarin photodimers in acetonitrile solution.[8] As the field of photoinduced single-crystal-to-single-crystal reactions is rapidly developing it is desirable to examine the occurrence of two-photon processes in single-crystal studies.

We describe here an X-ray crystallographic kinetic analysis of the two-photon dimerization of α-*trans*-cinnamic acid (**CA**) to α-truxillic acid (**TA**) (Scheme 1). The reaction remains one of the most studied solid state [2+2] photodimerizations since the pioneering studies of Schmidt and co-workers in the sixties established the topochemical principles governing such reactions.[9,10] In a recent study the kinetics of the one-photon induced dimerization of α-*trans*-cinnamic acid in microcrystalline powders were measured by using NMR $^{13}C$ cross-polarization magic angle spinning.[11] In the two-photon experiments of the current study, crystal orientation and the polarization of the laser light are fully controlled.

* Corresponding author. E-mail: jbb6@buffalo.edu and coppens@buffalo.edu.

**SCHEME 1: Photodimerization of α-*trans*-Cinnamic Acid to α-Truxillic Acid**

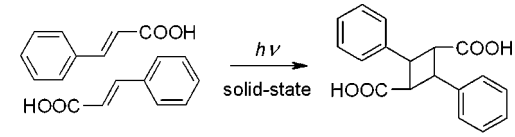


α-*trans*-cinnamic acid  α-truxillic acid

## Experimental Section

**Experimental Details.** *Crystal Growth and Preparation.* Single crystals of α-*trans*-cinnamic acid (TCI America) suitable for photodimerization and X-ray diffraction were obtained by slow evaporation from acetone. They belong to the monoclinic space group $P2_1/n$, with cell dimensions $a = 5.6283(2)$ Å, $b = 17.9569(8)$ Å, $c = 7.7399(3)$ Å and $\beta = 96.844(1)°$ at 280 K. While crystals typically grow as extended thin (010) plates, cleaving a large thick plate to a suitable size introduced multiple fracture lines that propagated throughout the crystal during laser irradiation resulting in undesirable polycrystalline diffraction patterns. Therefore smaller thick prisms were selected for the experiments, typically measuring 150 to 200 $\mu$m along each edge of (010) and being 75 to 100 $\mu$m thick. The (010) face of a **CA** crystal was mounted on the side of a glass fiber with a minimal amount of epoxy ensuring a clean opposite (010) surface for laser irradiation.

***X-ray Data Collection.*** X-ray diffraction data were collected at 280 K, using a Bruker SMART APEX2 CCD diffractometer installed at a rotating anode source (Mo Kα, $\lambda = 0.71073$ Å) and equipped with an Oxford Cryosystems nitrogen gas flow apparatus. The oscillation method ($\omega$-scan, 180°/scan, 0.5°/frame) was used in data collection. Typically, five full $\omega$-scans were collected before exposure, whereas two $\omega$-scans were performed after subsequent exposures.

***Laser Exposure.*** Crystals were irradiated with the second (532 nm) and third (355 nm) harmonics of a pulsed Nd:YAG laser (Continuum Surelite, 10 Hz, 1064 nm) with a pulse length of 5−7 ns. To ensure accurate normal incidence on (010), the crystal orientation was adjusted until the back reflection from

10.1021/jp809170t CCC: $40.75 
Published on Web 03/03/2009

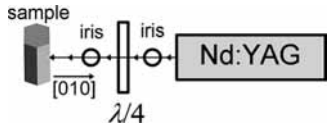


**Figure 1.** Schematic representation of the experimental arrangement for in situ laser-light exposure. The [010] direction of the crystal is parallel to the incident radiation.

this surface was parallel to the incident radiation. Circularly polarized radiation was generated by passing the linearly polarized laser output through a zero-order $\lambda/4$ waveplate (Newport, 10RP54-1) for 532 nm light or a multiorder $\lambda/4$ waveplate (Thorlabs, WPMQ05M-355) for 355 nm radiation (Figure 1).

**The Refinement of the CA Crystal Structure before Exposure.** The structure was solved by direct methods (SHELX97). All non-hydrogen atoms were refined anisotropically. The hydrogen atoms were located in the difference maps and assigned to ride on the parent atoms. Because of the similar lengths of the carbon−oxygen bonds (C1−O1 = 1.277 Å; C1−O2 = 1.256 Å) and the presence of two distinct appropriately located residual electron density peaks near the two oxygen atoms, the carboxylic acid proton was treated as being disordered. The occupancy for the disordered protons was constrained to sum to 1.0, leading to refined values of 65.4% and 34.6% for the protons connected to O1 and O2, respectively.

**The Refinement of the Partially Converted Crystal.** As the photochemical reaction proceeds, an increasing amount of truxillic acid (**TA**) is generated within the cinnamic acid lattice. Using a carefully constructed and rigorously tested two-component model that consists of a cinnamic acid molecule and half of a truxillic acid dimer in the asymmetric unit, the relative amounts of the two species in the lattice are determined from the occupancies of the two parts. The occupancy of the cinnamic acid fragment and the corresponding truxillic acid fragment were constrained to sum to 1.0.

The position of the atoms of the carboxylic acid group is complicated by the intrinsic disorder of the local chemical environment and could not be reliably refined in the multicomponent structure. As the chemical reaction proceeds, four distinct combinations of the $R_2^2(8)$ COOH dimer would be needed to be accounted for the model, they are the **CA**−**CA**, **CA**−**TA**, **TA**−**CA**, and **TA**−**TA** dimers. The non-hydrogen atoms of this group were assigned full occupancy while the protons were assigned half-site occupancy in each of the distinct positions. This ensures that the solution is not over parametrized and prohibits the intrinsic disorder of this group from biasing the calculated amount of **CA** and **TA** present.

The refinement of the reaction product in the final model was limited to six phenyl carbons, the two carbons α and $\beta$ to the COOH group and their associated hydrogen atoms. Several additional constraints and restraints were necessary to ensure the accuracy of the model. Corresponding atoms in the reactant **CA** and the product were constrained to have identical thermal parameters (command EADP in SHELX). Additional soft geometric constraints on distances (DFIX), angles (DANG) and coplanarity (FLAT) were employed to ensure that the minor species maintained a chemically sensible geometry. Without these constraints, the atoms in the minor species tended to drift toward the positions of the atoms in the major species. The universal application of these restraints prevents bias that would be introduced if the models in each data set were refined by using differing sets of restraints.

The resulting model represents a framework for accurately determining the changes in electron density as the reaction proceeds and thus the composition of the single crystal. The model is flexible enough to allow the two chemical components to adopt their proper position in the cell, which is critical given the large change in the $\beta$-angle as the reaction proceeds, yet this model possesses the rigidity to allow distinction between the two species.

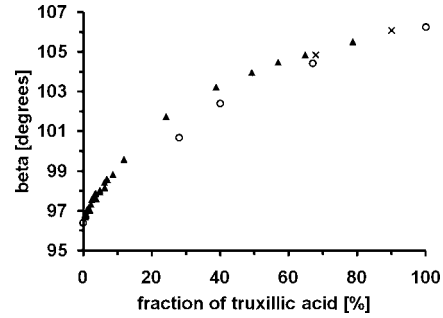


**Figure 2.** Plot of the fraction of α-truxillic acid versus $\beta$: open circles, ref 13; crosses, ref 12; triangles, this work.

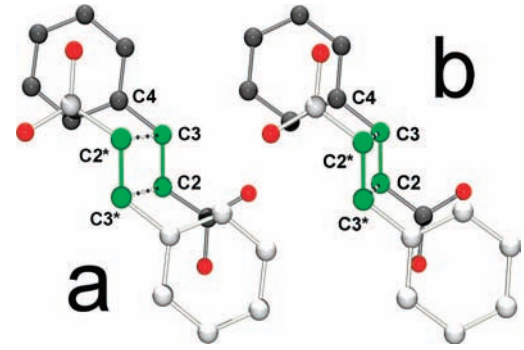


**Figure 3.** View of pairs of cinnamic acid molecules normal to the C2−C3−C4 plane which contains the reactive double bond (highlighted in green) prior to dimerization (a) and in a crystal that is 79% converted to α-truxillic acid (b). Dashed lines between the molecules highlight the improvement in overlap between the reacting atoms.

**Theoretical Calculations.** The B3LYP functional and the 6-31G* basis set of Gaussian 03 were used in the geometry optimization and subsequent calculation of the transition moments for the first ten electronic excitations of *trans*-cinnamic acid. The atomic coordinates from a **CA** structure including only the proton with the larger occupancy (H1) were selected as the starting geometry in the optimization.

## Results

**Monitoring the Photoreaction.** As shown in Figure 2 and in agreement with observations of Abdelmoty et al.,[12] a dramatic change in the $\beta$ angle from $\beta < 97°$ to $\beta > 106°$ in a crystal fully converted to α-truxillic acid accompanies the photodimerization of α-*trans*-cinnamic acid. The increase in $\beta$ as α-truxillic acid is formed is consistent and allows for a qualitative assessment of the progress of the reaction from the observed unit cell dimensions.

The change in the $\beta$ angle as the reaction proceeds improves the $\pi$-orbital overlap between juxtaposed pairs of cinnamic acid molecules. Figure 3, which is a view perpendicular to the molecular plane of **CA**, illustrates the large molecular shift required for the cyclobutane formation, which is the driving force for the pronounced change in the $\beta$-angle on reaction.

The [2+2] cycloaddition is initiated by a $\pi$ to $\pi^*$ HOMO to LUMO transition with an oscillator strength calculated as 0.70. The electronic dipole transition moment vector (EDTM) is approximately parallel to the long axis of the molecule, as

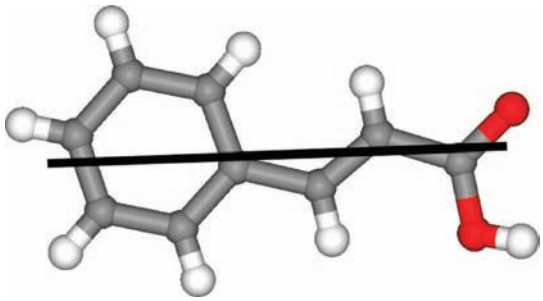

**Figure 4.** The transition moment for the lowest energy transition with the greatest oscillator strength (black line) superimposed upon the ground state structure of cinnamic acid used in the transition moment vector calculation.

illustrated in Figure 4. Neglecting possible rotation of the incident light in the crystal, the probability of excitation by photons with appropriate energies is proportional to $\cos^2 \theta$, where $\theta$ is the angle between the electric vector of the incident radiation and the EDTM.

As the cinnamic acid molecules project on (010) in a parallel orientation (Figure 5), polarized light propagating through the crystal perpendicular to this plane will experience highly anisotropic attenuation if the incident radiation is linearly polarized, as is the case for light from a Nd:YAG laser. To minimize the dependence of the absorption on the orientation around the normal to the (010) plane and therefore of the observed reaction rate, the laser light was converted into circularly polarized light as described in the Experimental Section. (Early experiments with linearly polarized light incident on (010) yielded remarkably inconsistent reaction rates, presumably due to the combination of the strong linear absorption anisotropy and the variation of the orientation of the crystal about (010).)

**Analysis of the Kinetics of the Reaction.** ***Reaction Rate As a Function of Length of Exposure.*** Figure 6 shows the fraction of α-*trans*-cinnamic acid converted to α-truxillic acid in a single crystal as a function of total time of exposure to 532 nm pulsed laser light. Each data point represents the fraction converted as determined by least-squares refinement of the structure after exposure for the time indicated. In agreement with previous NMR studies with 280−400 nm light from a Xe lamp,[11] the resulting curve has a sigmoidal shape, rather than exhibiting linear-, single-, multi-exponential or inverse time behavior, as is typically observed for solution reactions. Hayes *et al*. noted that this result is indicative of JMAK kinetics (Johnson, Mehl, Avrami, and Kolmogorov).[11]

In the JMAK model the kinetics of a phase transition involving a nucleation and growth mechanism is described by the equation[14−17]

$$y = 1 - e^{-kt^n}$$

where $y$ is the fraction of photoproduct formed in time $t$, $k$ is the growth rate constant, and the Avrami exponent $n$ is the dimensionality of growth of the nucleus: $n = 2$ for one-dimensional growth, $n = 3$ for two-dimensional growth, and $n = 4$ for three-dimensional growth. For a homogeneous reaction in which the probability of the reaction to occur is equal for any region within the sample for a given time interval, $n = 1$.[14−16] The experimental curve in Figure 6 corresponds to an Avrami exponent of 1.43 ± 0.08.

***Reaction Rate As a Function of Photon Flux.*** To confirm that irradiation with 532 nm light is a two-photon process, the dependence of reaction rate with photon flux must be measured.

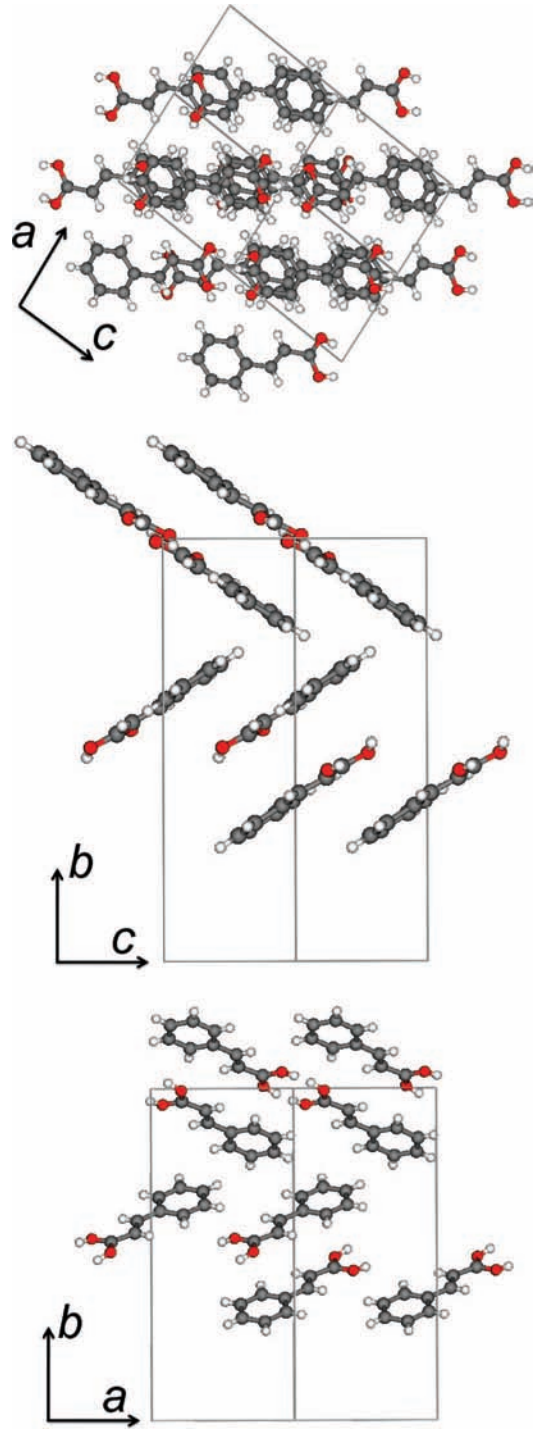


**Figure 5.** Crystal structure of α-cinnamic acid viewed along [010] (upper), [100] (middle), and [001] (lower).

To avoid possible deviations due faster growth of the nuclei once formed, we compared growth rates in the 0−10% conversion region, in which rates are close to linear (Figure 6), in a series of experiments with different photon flux. As before, the light beam is incident on (010).

As shown in Figure 7, initial photoconversion rate measurements on seven different crystals at various laser powers exhibit a nearly quadratic dependence on the flux of the incident 532 nm radiation. A plot of the logarithm of the conversion rate vs the logarithm of the photon flux is shown in the inset of Figure 7. The linear fit has a slope of 2.24 ± 0.18, within experimental error of the value of 2 expected for a two-photon process, thus

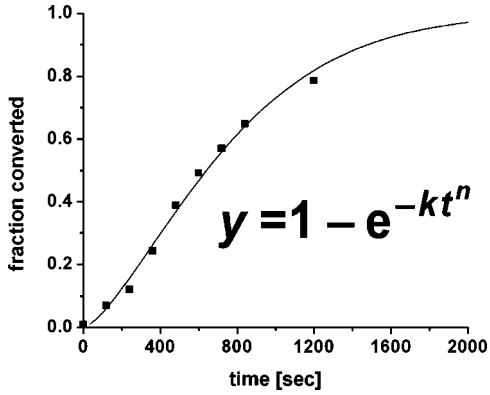


**Figure 6.** Plot of the fraction of α-*trans*-cinnamic acid converted to α-truxillic acid as a function of total irradiation time with use of 532 nm radiation. Data points (black squares) are based on refined occupation parameters from unique crystal structures. The black line is a fit to the data using the inset equation where $n = 1.43 \pm 0.08$ and $k = 6.7 \times 10^{-5} \pm 3.7 \times 10^{-5}$ s$^{-1}$.

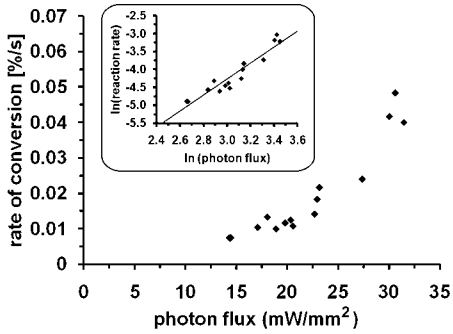


**Figure 7.** Plot of the rate of photoconversion of α-*trans*-cinnamic acid to α-truxillic acid as a function of 532 nm photon flux incident on (010). Inset: ln−ln plot. The slope of the fitted line is 2.24 ± 0.18.

confirming that the dimerization reaction initiated by 532 nm light is indeed a two-photon process.

As further discussed below, attempts to measure single-crystal reaction rates by using the one-photon "tail irradiation" technique described by Enkelmann and Wegner,[13] and reproduced by us, were not successful when applied to a single crystal in a fixed orientation. Regardless of incident laser power, 355 nm photons incident on (010) were strongly absorbed at the surface of the crystal resulting in disintegration as evidenced by a deterioration of the diffraction pattern upon irradiation. In one instance, however, two distinct diffraction patterns were observed.

A closer inspection of the crystal under a microscope revealed that the crystal splits approximately parallel to (010) forming two distinct plates of approximately equal thickness. These "front" and "back" plates were carefully separated and subjected to additional X-ray analysis. While reliable structure determinations could not be made, the diffraction patterns of each were successfully indexed. The unit cell of the "front" plate, the plate directly exposed to the incident laser radiation, was $a = 5.722(1)$ Å, $b = 18.853(4)$ Å, $c = 7.709(2)$ Å, $\beta = 104.925(6)$ Å. The unit cell of the "back" plate, the plate initially glued to the glass capillary, was $a = 5.6120(6)$ Å, $b = 18.273(2)$ Å, $c = 7.7081(8)$ Å, $\beta = 98.879(3)$ Å. Comparison of the $\beta$ angles with the results shown in Figure 2 gives conversion percentages of the front and back plates as ∼70% and ∼10%, respectively, indicating clearly the nonhomogeneous exposure of the crystal sample.

While the fundamental chemical reaction that occurs in the crystal is identical for 355 and 532 nm light, the spatial propagation of the reaction in the crystal is markedly different. The pronounced heterogeneous nucleation observed by using the "tail irradiation" technique was surprising given the success of this technique reported earlier. There are, however, several critical differences between the irradiation methods described herein and previous reports.

Previous work involving the photoconversion of α-*trans*-cinnamic acid to α-truxillic acid was carried out on a sample of randomly oriented microcrystals[12] or microcrystalline powders[11] using filtered broadband light sources or lasers with unspecified polarizations. While "tail irradiation" undoubtedly increases the penetration depth of the incident radiation, scattering from neighboring crystals and the container ensures crystals are irradiated from many different directions simultaneously. Such a condition is certainly obtained in the several instances in which the samples were stirred during irradiation.

The orientation of the crystal with respect to the primary light source also plays an important role in these experiments. Because the absorption coefficient of the crystal varies with the orientation, principal irradiation along a weakly absorbing direction will increase the penetration depth and will likely result in a slower reaction rate compared to irradiation along a strongly absorbing direction for a crystal of equal size and shape leading to a more homogeneous reaction. It should be noted that the absorption coefficient will also vary with the polarization of the incident radiation affecting the reaction rates similarly.

While the preservation of single-crystallinity throughout the reaction is of little concern for NMR characterization, it is critically important for crystal structure determination. Unlike the experiments described here in which a single crystal was subjected to numerous irradiations in precisely the same orientation, in the studies described earlier, crystals deemed most suitable for structure determination were selected after each successive irradiation of a multi-crystal sample. While providing the best sample for a crystal structure analysis, the precise knowledge of the irradiation details for the selected crystal are not available.

***Discussion of the Reaction Kinetics.*** The Avrami exponent, determined to be $1.43 \pm 0.08$ in our experiments (Figure 6), provides a quantitative measure of the homogeneity of the photoproduct distribution within the lattice resulting from two-photon absorption. An Avrami exponent of exactly 2 indicates perfect one-dimensional growth from nuclei which form continuously and at a constant rate throughout the reaction. Using broadband UV radiation of 280−400 nm, Bertmer *et al.* determined an Avrami exponent of $1.66 \pm 0.10$ and concluded the photoconversion mechanism followed one-dimensional growth of the nuclei with a decreasing rate of nucleation.[11] While a decreasing rate of nucleation can be responsible for Avrami exponents between 1 and 2, a similar value could result from a hybrid mechanism, combining a homogeneously occurring reaction ($n = 1$) and a growth of nuclei once formed, as described by a modified Avrami equation:

$$y = 1 - [A \cdot e^{-k_1 t}] - [B \cdot e^{-k_2 t^n}]$$

where $A$ and $B$ represent the relative importance of different mechanisms.

A physical basis for using nucleation and growth mechanisms to model the kinetics of the photodimerization can be found by examining the spatial relationship of the cinnamic acid molecules in the low conversion and high conversion crystal structures, illustrated in Figure 3. The probability that a [2+2] photodimerization reaction will occur upon electronic excitation is sensitive to the spatial overlap of the reacting $\pi$-orbitals: the greater the overlap, the higher the probability that the dimer-

ization will occur.[18] For a dimerizable pair of cinnamic acid molecules, the reactive double bonds are parallel, a consequence of the inversion symmetry relating the molecules, but are offset in directions parallel and perpendicular to the bond. As a single parameter to characterize the overlap of the bonds, we will use the offset angle, $\delta$, the angle between C2* and C3 (Figure 3), and the normal to the C2, C3, C4 plane. For perfect overlap, $\delta$ is equal to zero. In nonirradiated α-*trans*-cinnamic acid crystals $\delta$ is 18.4°, but in a crystal that has been 79% converted it is reduced to 10.9°.

Thus as the photodimerization proceeds, photodimerizable pairs are shifted into positions which increase the probability that they will react upon exposure. The shift should be most evident in the neighborhood of product truxillic acid molecules. Thus, although the initial product formation may be homogeneous in a uniformly exposed volume, additional product molecules may be formed preferentially in the neighborhood of existing dimers, leading to a deviation from homogeneous product formation, and an Avrami coefficient larger than 1, as observed.

## Concluding Remarks

The experiments described above confirm that the single-crystal dimerization of α-*trans*-cinnamic acid can take place through two-photon excitation when a high powered Nd:YAG laser with ~10 ns pulse width is used. The two-photon technique has the great advantage of much better penetration of light in the single crystal, and therefore more homogeneous product formation. It avoids formation of a fully converted surface layer at an early stage of exposure, which often blocks exposure of the bulk of the sample. The kinetics of the reaction on increasing exposure fits the JMAK expression with a coefficient indicating a mechanism that is intermediate between random distribution of product molecules in the crystal, which would lead to first-order kinetics, and faster dimerization after product-induced distortion of the lattice. The use of two-photon excitation in time-resolved diffraction experiments is to be investigated in subsequent studies.

**Acknowledgment.** We thank Dr. Shao-Liang Zheng for stimulating discussions. This work was supported by the National Science Foundation under grant CHE0236317.

**Supporting Information Available:** CIF file for α-*trans*-cinnamic acid. This material is available free of charge via the Internet at http://pubs.acs.org.

## References and Notes

(1) Harada, J.; Uekusa, H.; Ohashi, Y. *J. Am. Chem. Soc.* **1999**, *121*, 5809–5810.
(2) Harada, J.; Nakajima, R.; Ogawa, K. *J. Am. Chem. Soc.* **2008**, *130*, 7085–7091.
(3) Naumov, P.; Sekine, A.; Uekusa, H.; Ohashi, Y. *J. Am. Chem. Soc.* **2002**, *124*, 8540–8541.
(4) Coppens, P. (Focus article). *Chem. Commun.* **2003**, 1317–1320.
(5) Coppens, P.; Vorontsov, I. I.; Graber, T.; Gembicky, M.; Kovalevsky, A. Y. *Acta Crystallogr.* **2005**, *A61*, 162–172.
(6) Coppens, P.; Zheng, S.-L.; Gembicky, M. *Z. Kristallogr.* **2008**, *223*, 265–271.
(7) Bhawalkar, J. D.; He, G. S.; Prasad, P. N. *Rep. Prog. Phys.* **1996**, *59*, 1041–1070.
(8) Kim, H. C.; Kreiling, S.; Greiner, A.; Hampp, N. *Chem. Phys. Lett.* **2003**, *372*, 899–903.
(9) Cohen, M. D.; Schmidt, G. M. J.; Sonntag, F. I. *J. Chem. Soc.* **1964**, 2000–2013.
(10) Schmidt, G. M. J. *J. Chem. Soc.* **1964**, 2014–2021.
(11) Bertmer, M.; Nieuwendaal, R. C.; Barnes, A. B.; Hayes, S. E. *J. Phys. Chem. B* **2006**, *110*, 6270–6273.
(12) Abdelmoty, I.; Buchholz, V.; Di, L.; Guo, C.; Kowitz, K.; Enkelmann, V.; Wegner, G.; Foxman, B. M. *Cryst. Growth Des.* **2005**, *5*, 2210–2217.
(13) Enkelmann, V.; Wegner, G. *J. Am. Chem. Soc.* **1993**, *115*, 10390–10391.
(14) Avrami, M. *J. Chem. Phys.* **1939**, *7*, 1103–1112.
(15) Avrami, M. *J. Chem. Phys.* **1940**, *8*, 212–224.
(16) Avrami, M. *J. Chem. Phys.* **1941**, *9*, 177–184.
(17) Christian, J. W. *The theory of transformations in metals and alloys, Part I*; Elsevier Science Ltd: Oxford, UK, 2002; Vol. I.
(18) Kearsley, S. K.; Desiraju, G. R. *Proc. R. Soc. London, A* **1985**, *397*, 157–181.

JP809170T